NCRA • TIFR

A Look at GMRT Tracking Accuracy

Divya Oberoi and Manisha Jangam

Email:div@ncra.tifr.res.in, manisha@gmrt.ncra.tifr.res.in

Objective: To examine GMRT tracking accuracy by examining the difference between the target and the actual positions of the GMRT antennas, as reported by the servo system while in tracking mode.

Revision	Date	Modification/ Change	
Ver. 1	27 July 2015	Initial Version R-262	1

Contents

1 Introduction and Motivation

The tracking accuracy of GMRT is generally believed to be one of the factors limiting GMRT performance. With the increased sensitivity of the uGMRT system, it will only become more important to understand this limitation. Here we take a quantitative look at the tracking errors as reported by the GMRT servo system, to build a sense for the magnitude and nature of the problem.

Traditionally tracking and pointing accuracies of about $1/10^{th}$ to $1/20^{th}$ of the HPBW at the frequency of operation have been regarded as sufficient. For a given telescope, the tightest constraints naturally come from the highest observing frequency. In the case of GMRT, the HPBW at 1280 MHz is about 26 arcmin. Consistent with the then prevalent norms, the original target specification of the GMRT servo system was to provide a tracking and pointing accuracy of 1 arcmin for wind speeds less than 20 kmph (Chap. 20, Low Frequency Radio Astronomy, 2003, Eds. Chengalur, Gupta and Dwarkanath).

A time varying tracking error leads to a change in the observed flux density of a source as a function of time. These varying fluxes densities lead to deconvolution errors during the imaging process. The sources affected the most by such errors are the ones sampled by the part of the antenna beam where its gradient is large. This gradient tends to be large in a fairly
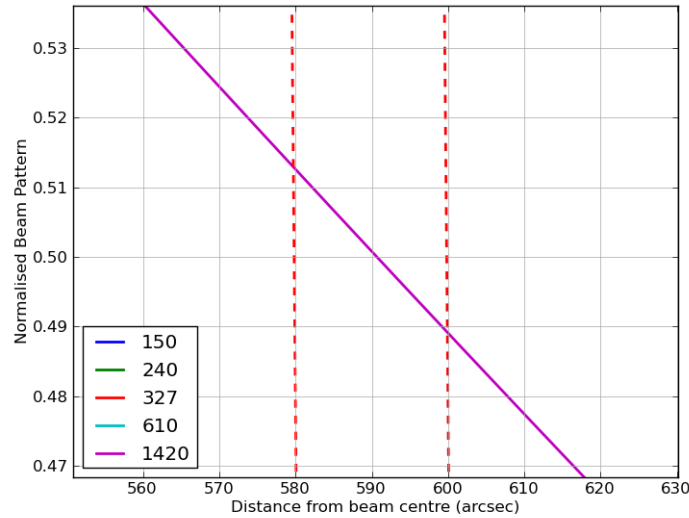
Figure 1: The figure shows a cut across the GMRT beam at 1420 MHz around the HPBW point. The vertical dashed lines in the right panel mark ±10" from the HPBW point. At 1420 MHz, a tracking error of ±10" corresponds to a change of about 1 % in the gain of the beam.

large region around the HPBW point. An illustration is shown in Fig 1. A tracking error causes the flux of the sources in about one half the beam to increase and in about the other half to decrease. The magnitude of this increase or decrease is a function of the direction of the tracking error and the distance of the source from the fiducial beam center. Tracking errors have both systematic and random components, the latter can arise from causes ranging from an under-damped servo system to gusts of wind.

At present the information of tracking error is not routinely provided by most observatories. We note that none of the standard interferometric analysis packages have the ability to correct for it even if the tracking error information were available.

2

2 Data used and procedure

The ONLINE log records detailed information about the state of the GMRT antennas (and downstream signal chain **True?**). These logs are available since August 2009. We used servo data from the ONLINE database when servo flag is set to tracking and abs(EL/AZ tacho) < 100. Here we present our results from examining one day of data, the 20th of July, 2012 and 5 days in December 2012. The day in July was chosen because it was windiest day of 2012 and wind gusts are expected to give rise to larger tracking errors.

The ONLINE database provides information of the *target position* (TP) and the *current position* (CP) for azimuth and elevation axes for each of the antennas with a time sampling of ∼6 seconds. The tracking error in elevation (TE_{el}) is defined as:

$$TE_{el}(t) = TP_{el}(t) - CP_{el}(t), \tag{1}$$

and the tracking error in azimuth (TE_{az}) is defined as:

$$TE_{az}(t) = \{TP_{az}(t) - CP_{az}(t)\} \times Cos(el), \tag{2}$$

where el is the elevation angle of the antenna in radians at the time of the measurement.

Histograms of tracking errors for both the elevation and the azimuth axes for all antennas were examined. The tracking errors for C00 are shown on a linear and a log scale in Fig. 2. Figure 3 shows the azimuth and elevation tracking errors for all of the GMRT antennas. This figure shows that the tracking errors most of the GMRT antennas are very similar and also well behaved. We also examined tracking errors as a function of the wind speed, an example is shown in Fig. 4.

We also looked for dependence of tracking errors on the location of the antenna itself by examining plots of azimuth (elevation) tracking errors as a function of azimuth (elevation). An example of such a plot for C00 is shown in Fig. 5. The plot shows a hint of change in distribution of tracking errors for azimuths <100° and >100°. In order to get more data points and a better sampling of the azimuth axes, we repeated the exercise combining 5 neighbouring days of data (8, 9, 15, 16 and 29 Dec, 2012) from a part of the year when winds are usually quite low. Figure 5 also includes the plot for these data. The change in distribution of azimuth tracking errors is evident in this plot as well.
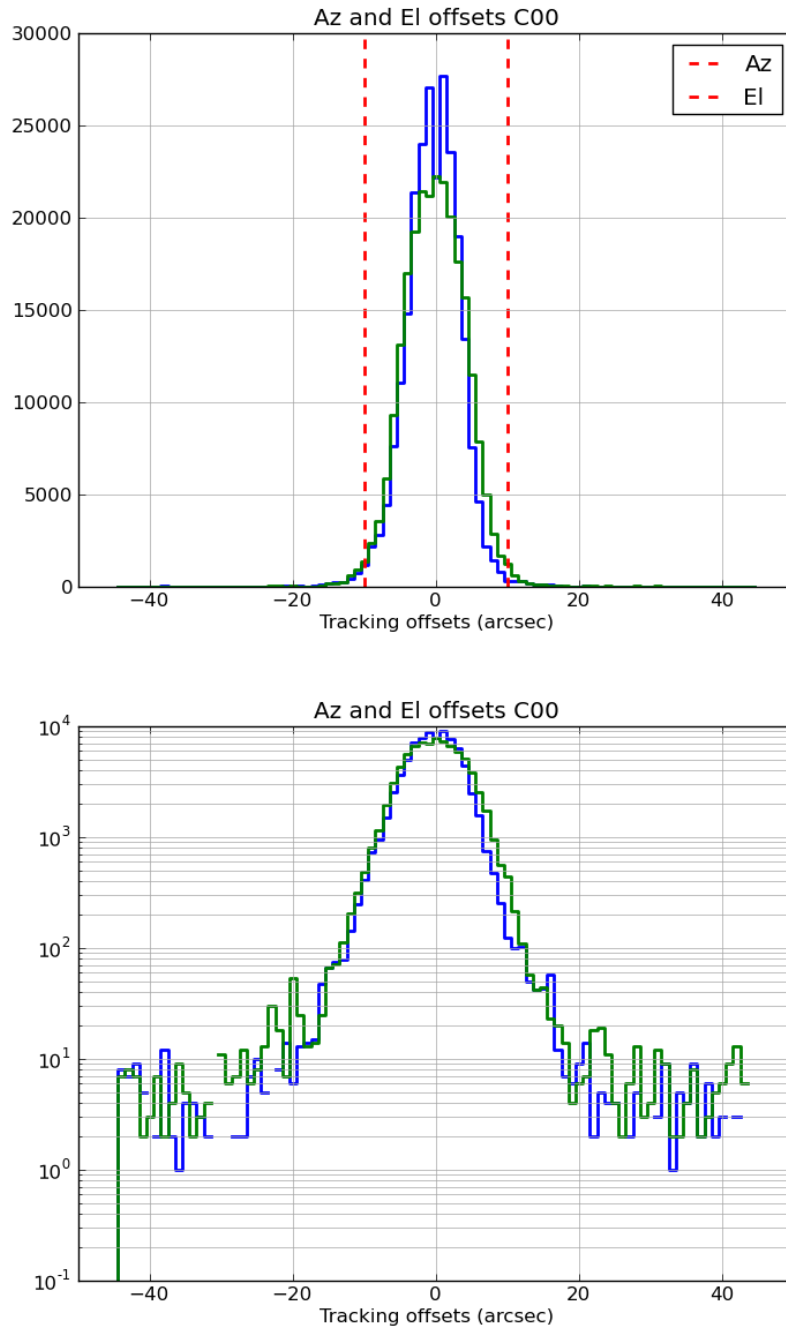
3

Figure 2: Histogram of tracking errors for C00 along the azimuth (blue) and elevation (green) axes. The top panel in on a linear scale and the lower panel on a log scale. The vertical dashed lines mark ±10". The FWHM of the histogram is ∼9".
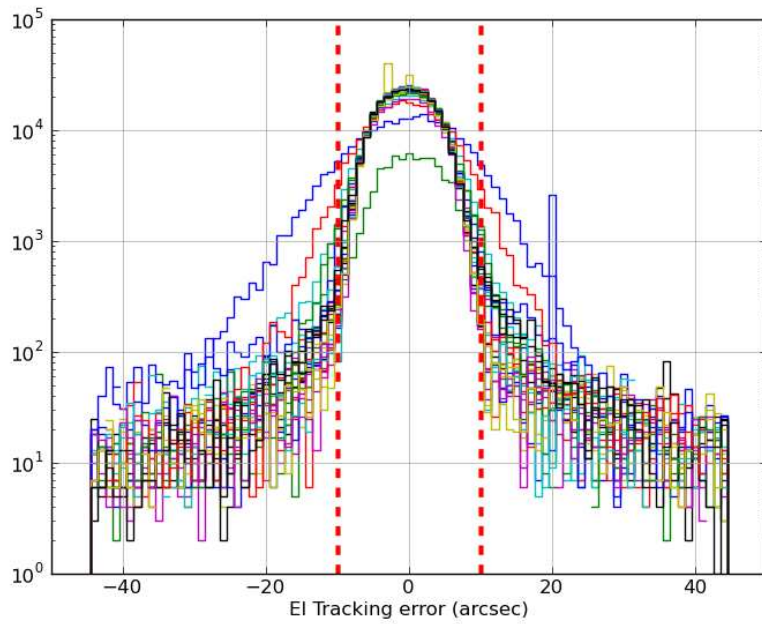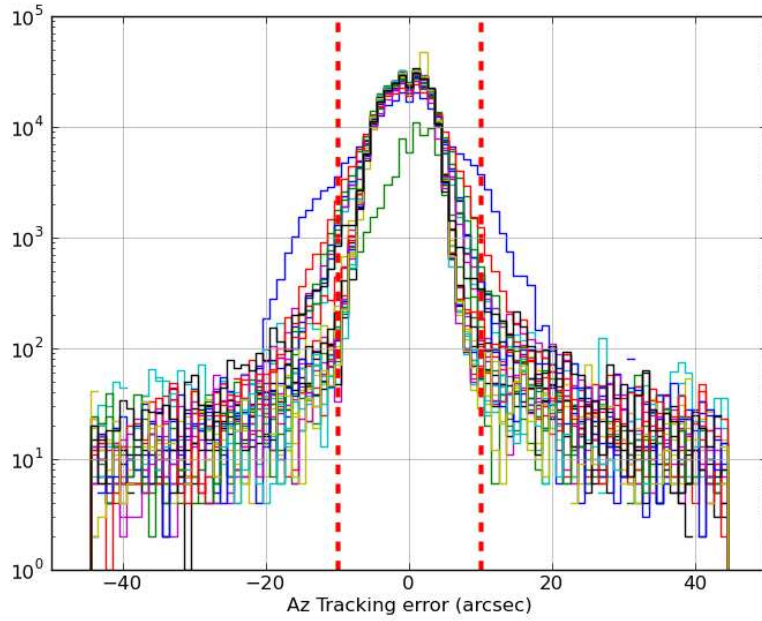
Figure 3: The top and bottom panels show the azimuth and elevation tracking errors, respectively, for all the GMRT antennas. The vertical dashed lines mark ± 10".
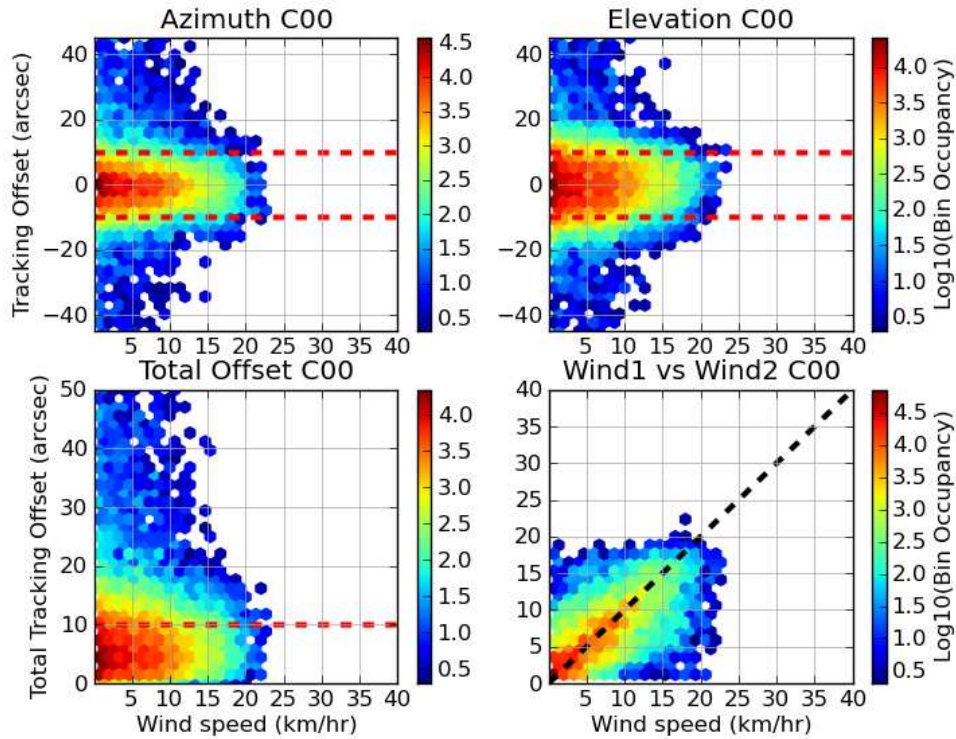
5

Figure 4: The tracking error data for C00 is presented as an example. The x axis in all panels shows wind speed in km hr^{-1}. The y axis on the top two panels shows tracking errors for the azimuth (left) and the elevation (right) axis, respectively. On the bottom left panel the y axis shows the total tracking error, obtained by combining the azimuth and elevation tracking errors in quadrature. The horizontal dashed lines on all these panels mark ±10". The bottom right panel is a consistency check between the two anemometers on C00. It plots the wind speed measured by one instrument against that measured by the other in km hr^{-1}. The diagonal dashed line marks x=y. All the panels show two dimensional histograms and the colour represents the bin occupancy on a log$_{10}$ scale.

6

Plots for all the GMRT antennas in the formats shows in Figs. 4 and 5 are presented in Appendix A. As noted in Sec. 3, the dependence of tracking errors on wind speed was not discernible in this analysis. Hence for the purpose of figures in Appendix A, we have chosen to plot data or the same five days from December 2012 as mentioned in the earlier paragraph, rather than the windiest day of 2012.

3   Results

This approach provides a robust estimate of the tracking performance of the servo system. The key results from this study are:

1. As estimated from the data, the servo tracking errors for most antennas are found to be within $\pm$ ~5" in azimuth and $\pm$ ~6" in elevation. Tracking errors of this magnitude can lead to fluctuations in the apparent flux density of ~0.5% or smaller at 1420 MHz (Fig. 1). Pleasantly, these tracking errors are much smaller than the system performance specifications of ± 1', originally laid down for the servo system.

2. Based on the admittedly limited data examined here, there does not seem to be any evidence for the tracking errors to be increasing with wind speed.

3. There is some hint for the azimuth tracking errors having a slight dependence on the absolute position of the antenna. The peak of the azimuth tracking error histogram seems to be at a small -ve number in the range -100°–100°, and a at small +ve number outside this range.

We noticed a few anomalies in the coarse of this work. They are listed below:

1. **C01** : Azimuth tracking error histogram significantly broader than the average. One of the anemometers not working.

2. **C00** : A broader than average tracking error histogram in both elevation and azimuth axes.

3. **C02** : A slightly broader than average tracking error histogram in the elevation axis.
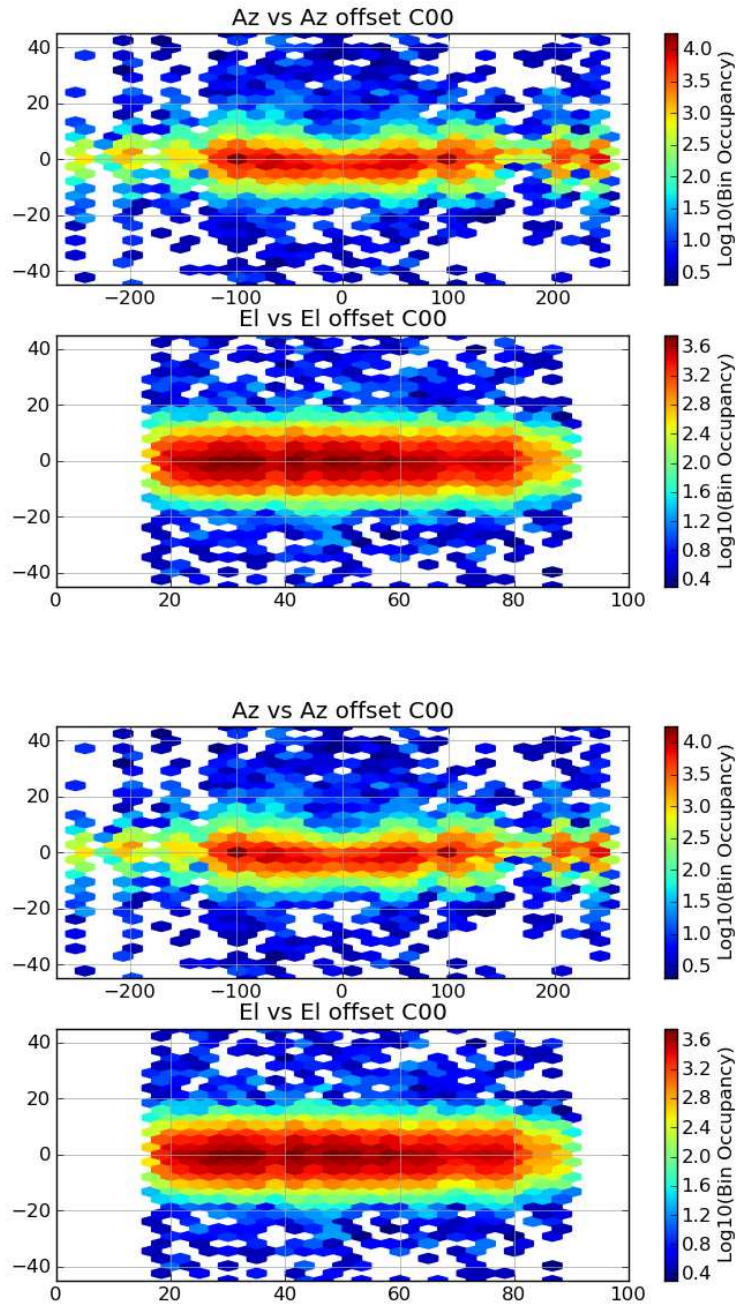
Figure 5: The top two panels shows the azimuth and elevation tracking errors for C00 as a function of azimuth and elevation, respectively, of the dish. These panels show data corresponding to one day. The bottom two panel are in the same format as the top two and combine data from five neighbouring days. All the panels show two dimensional histograms and the colour represents the bin occupancy on a $\log_{10}$ scale.

4. **C04** : A broader than average tracking error histogram in the elevation axis.

5. **C10** : A broader than average tracking error histogram in both elevation and azimuth axes.

6. **C14** : A broader than average tracking error histogram in both elevation and azimuth axes.

7. **E02** : The two anemometers show practically identical readings, unlike most others.

8. **E05** : The two anemometers show practically identical readings, unlike most others.

9. **S06** : Shows a wide pedestal in the azimuth tracking error histogram. From the lowest panel of Fig. 17 it is evident that this large spread comes from the elevation range $\pm$ 10° around 45°.

10. **W03** : One of the anemometers is not working.

11. **W05** : No data.

12. **W06** : A larger spread in the elevation tracking errors between elevation angle 30° − 70°.

4 Limitations of the present work

We recognise the following limitations of the present work:

1. The servo system is expected to be able to cope with the steady component of the wind speed. It is the wind gusts on significantly smaller time scales which are likely to give rise to large tracking errors. The ONLINE database currently has a cadence of ∼6 s, much coarser than the sampling needed (order 100 ms) to estimate this effect. We do not appreciate the details fully, but we were given to understand that the wind speed reported by the anemometers is an average over some duration (presumably a few s), so the wind data available in the ONLINE database might be of limited utility in identifying periods of strong wind gusts.

2. From an astronomer's perspective, the relevant pointing error will also include the residual pointing error from the pointing model, which should include the impact of gravitational distortion of the antenna structure. Our analysis is insensitive to these errors.

3. The tracking errors as defined here are useful for characterising the performance of the servo system. An actively driven antenna structure will distort and flex in response to the torques and forces applied on it by the servo system and the wind. These can lead to a distortion of the antenna beam, which is not addressed in this work.

5 Future work and utility

1. The M&C system for the uGMRT will allow the antenna state to be logged with a much faster cadence, though it might still not meet the needs of an experiment to estimate the impact of wind gusts on tracking errors. A dedicated setup to estimate is likely to be needed to quantify this.

2. The work presented here demonstrates that statistically stable quantitative information about tracking accuracies of GMRT antennas can be obtained by this approach. If it is regarded to be useful, quantitative estimates for FWHM/Gaussian σ of the histograms individual antennas can be provided. This sort of analysis provides a diagnostic which can be used to track antenna performance over time.

3. Comparing the wind speeds reported by the two anemometers on a given antenna is also a useful diagnostic for checking the health of these instruments. As we rely on the information from these instruments to make the decisions to stop observing and stow the dishes when the wind speed rises, it will be useful exercise to look for faulty anemometers before the start of the high wind season.

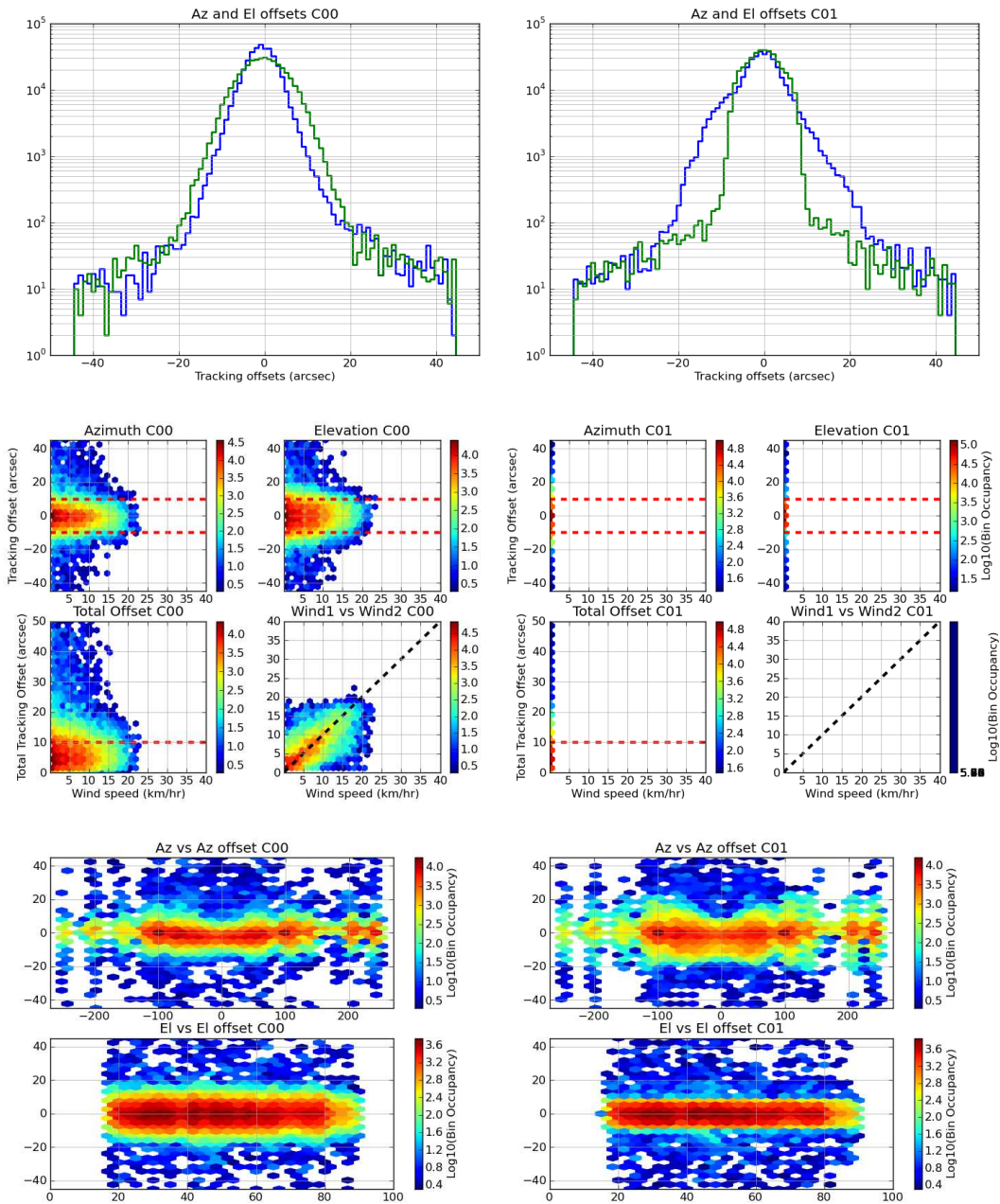# 6 Acknowledgments

A Plots for all GMRT antennas

Figure 6: The left and right panels shows the plots for C00 and C01, respectively. The top panels show the azimuth (blue) and elevation (green) tracking errors on a $\log_{10}$ scale. The middle and bottom panels are in the same format as Figs. 4 and 5, respectively.
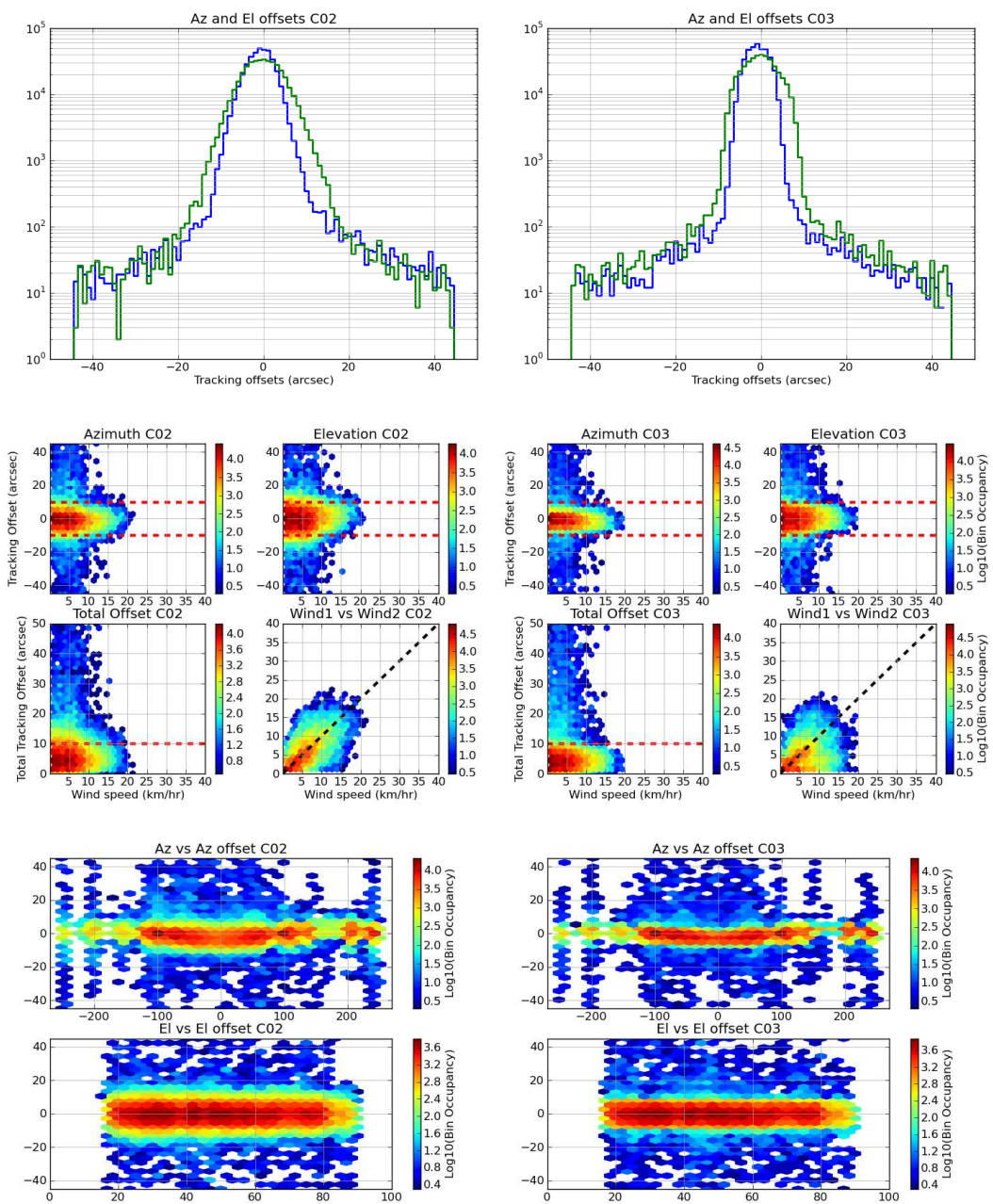
12

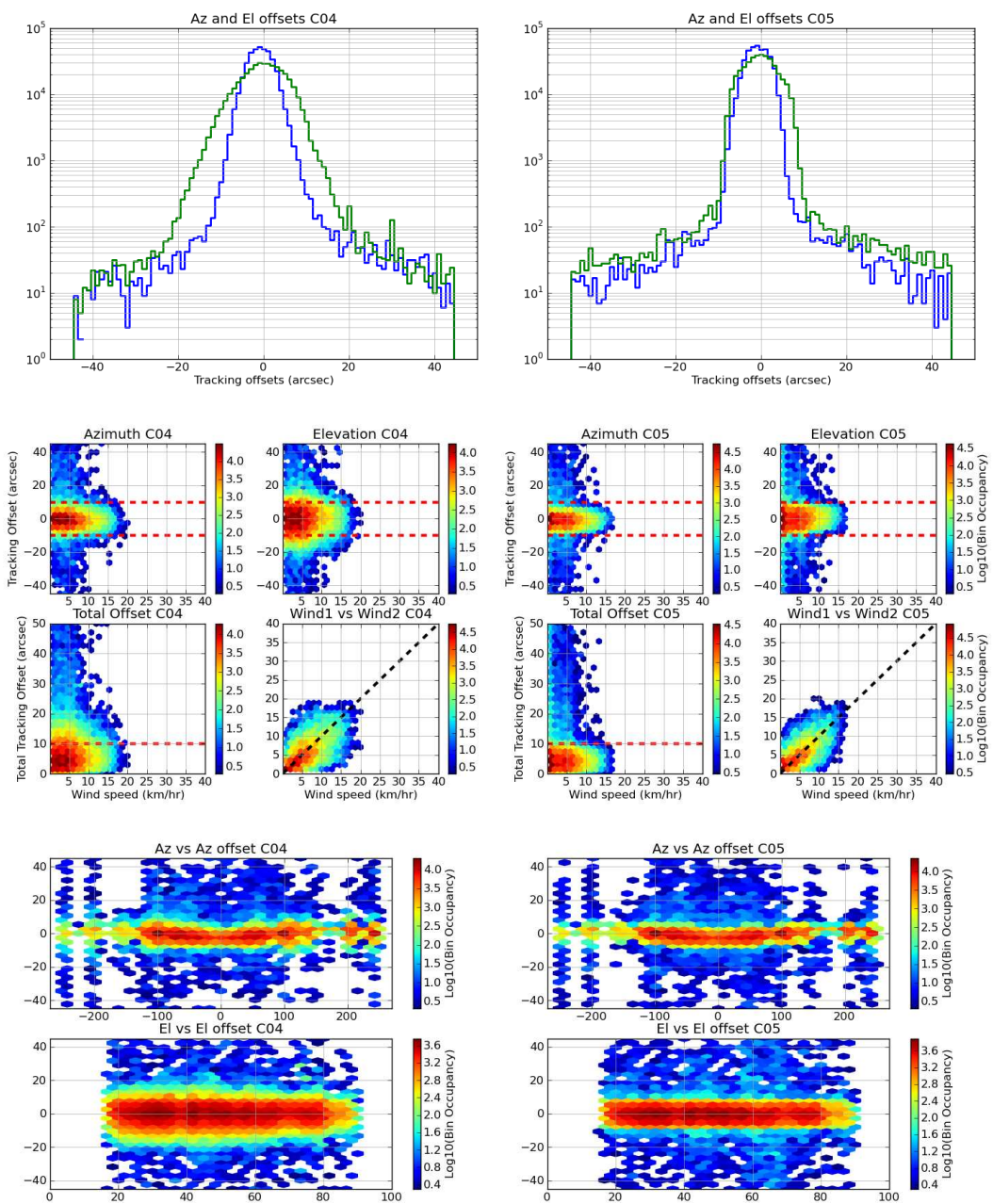Figure 7: Figures for C02 and C03 in the same format as Fig. 6.

13

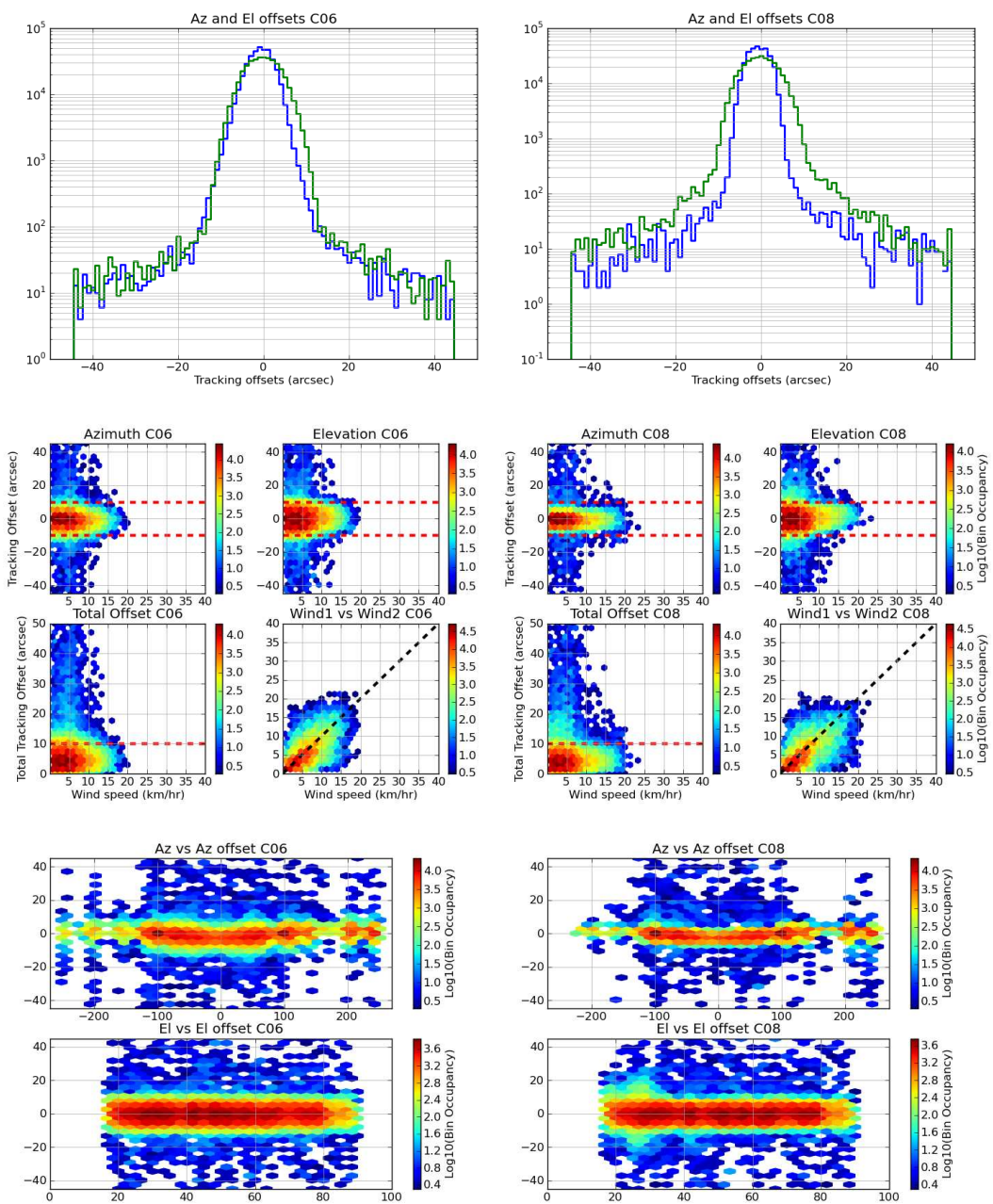Figure 8: Figures for C04 and C05 in the same format as Fig. 6.
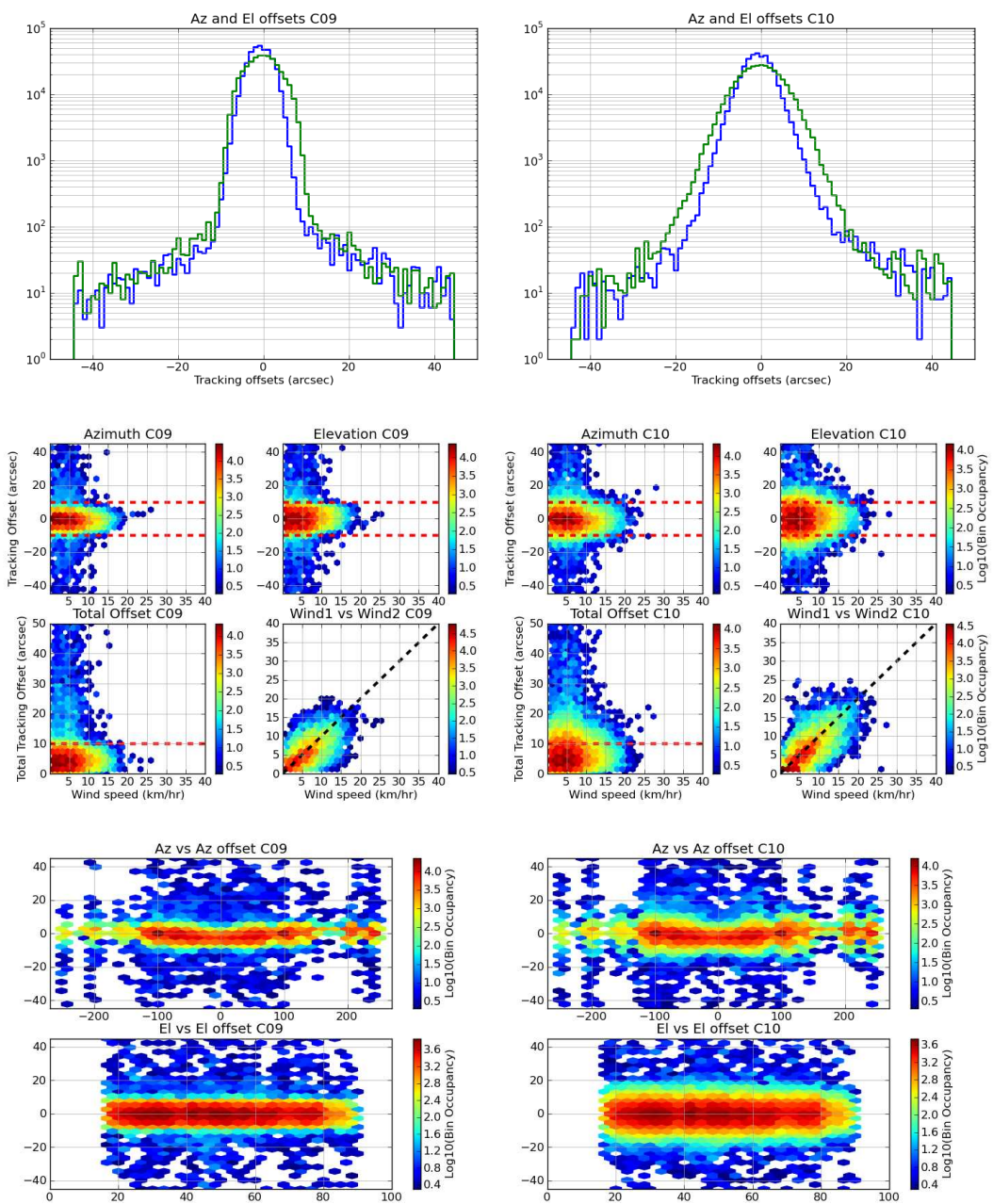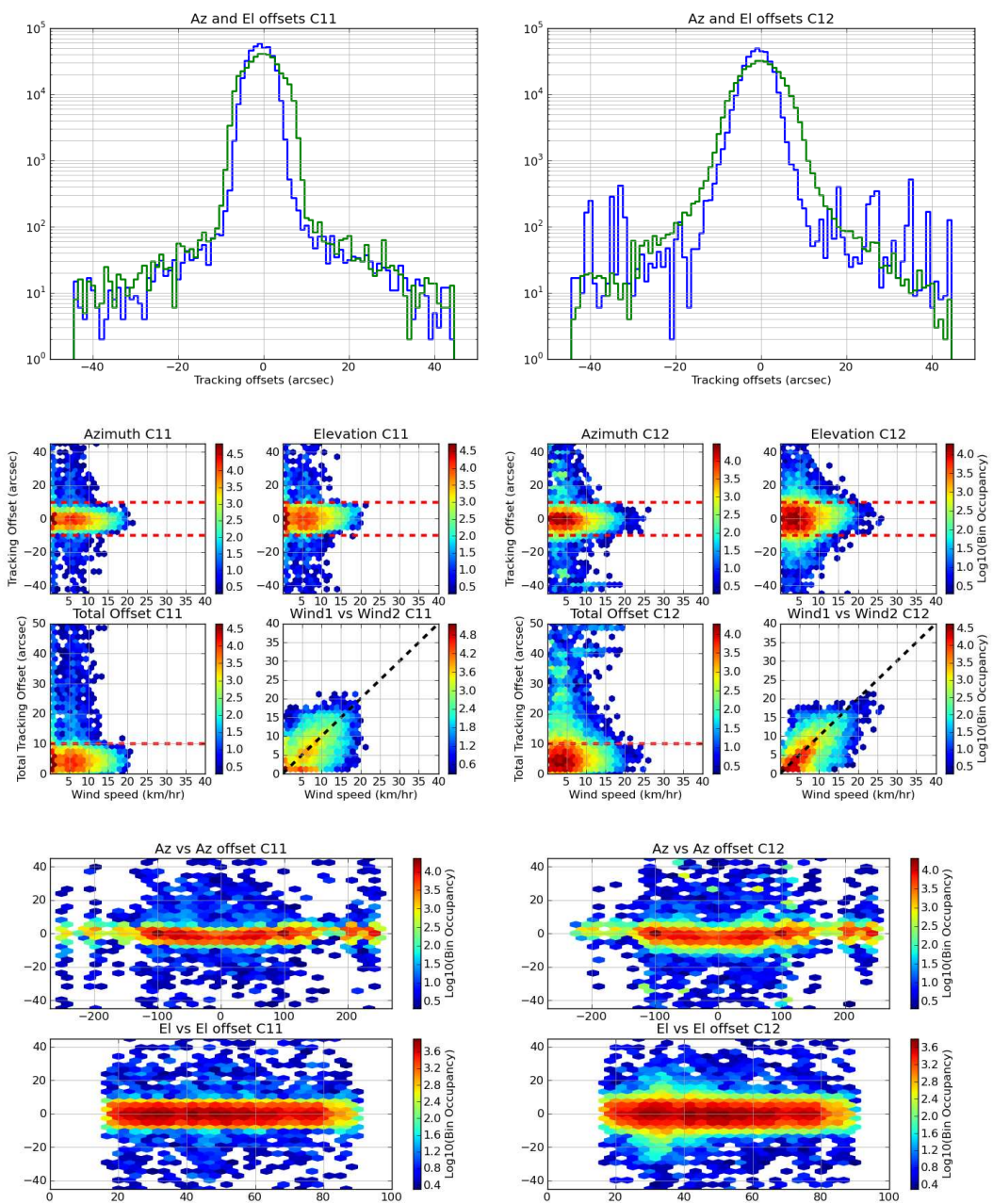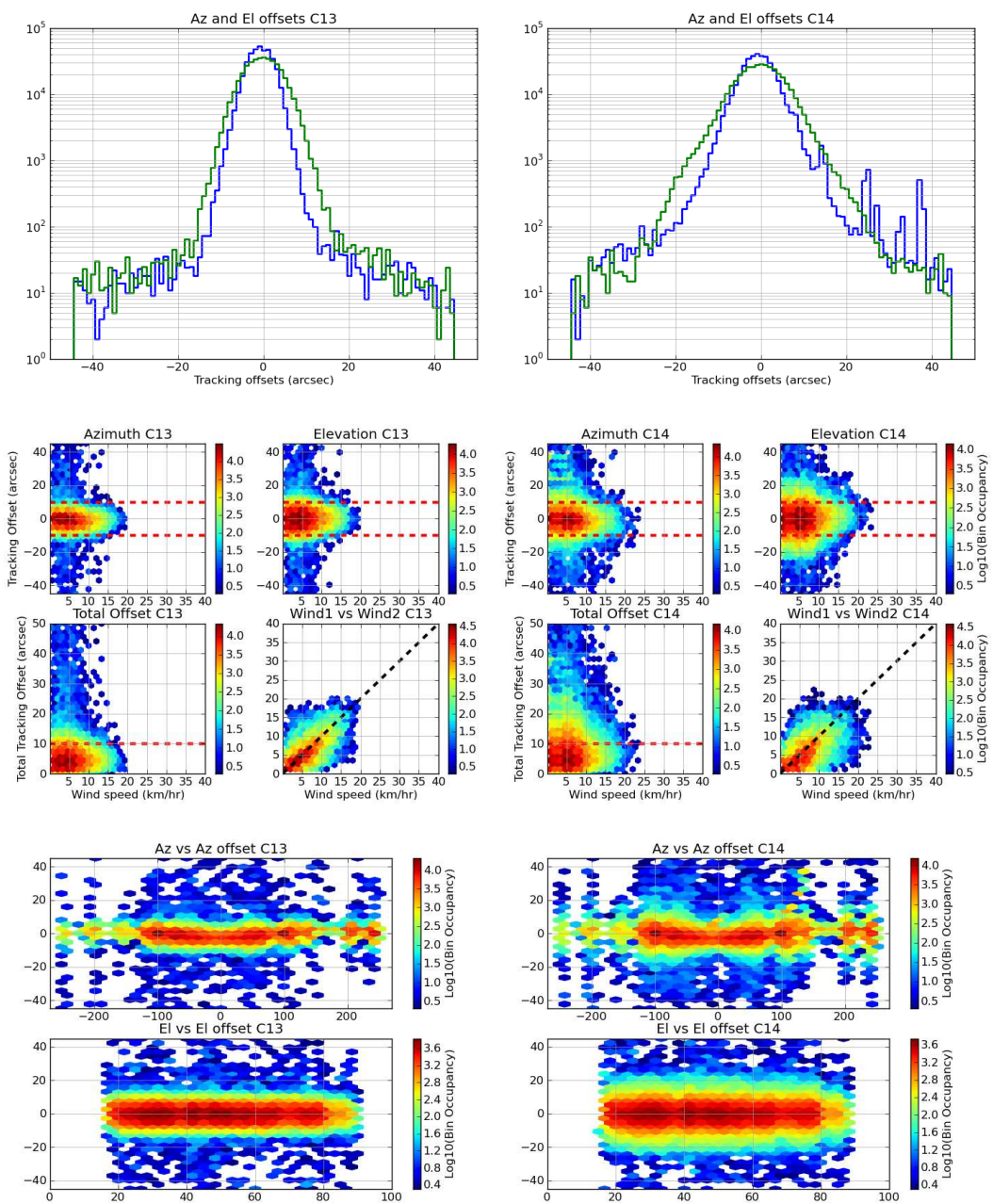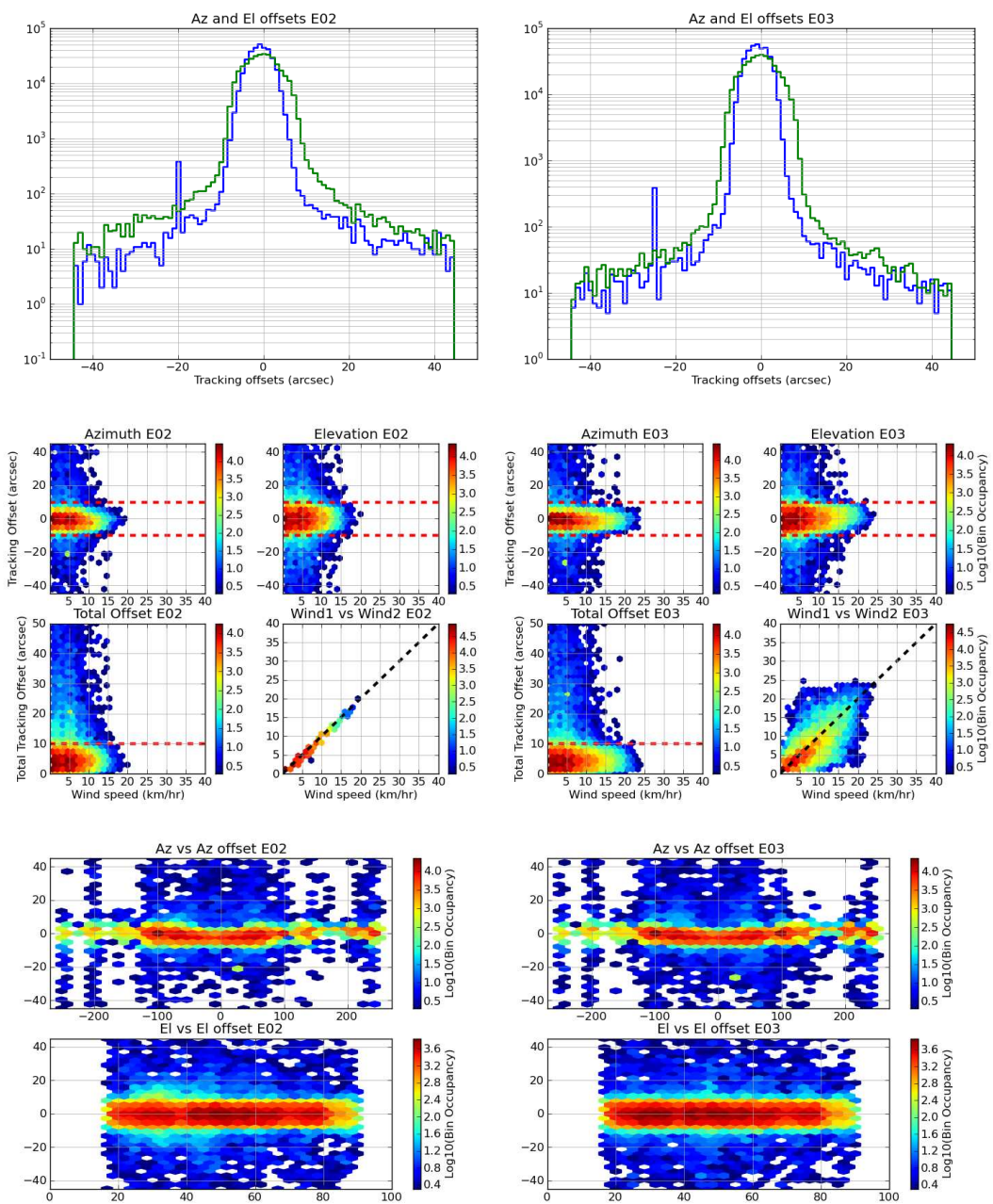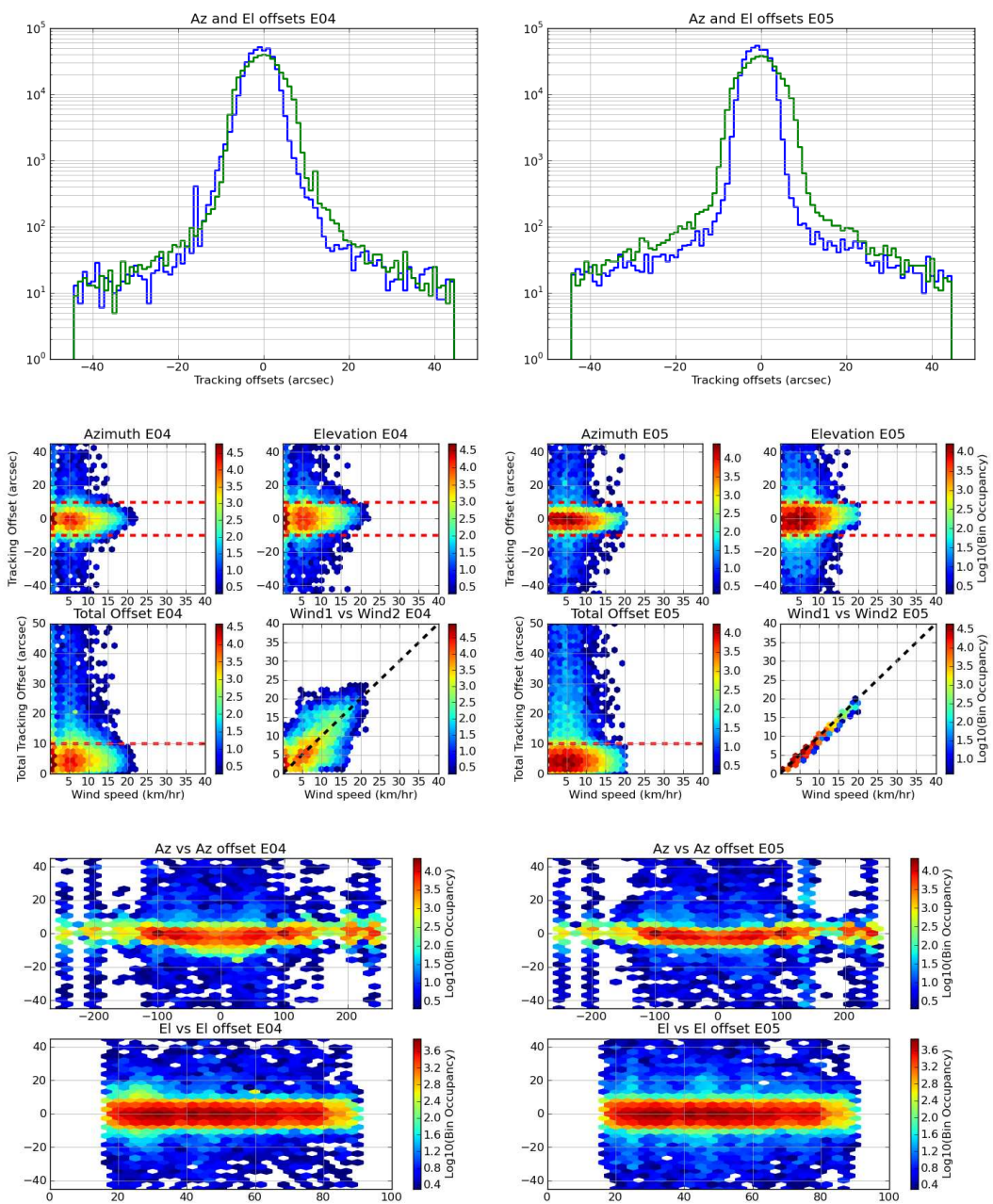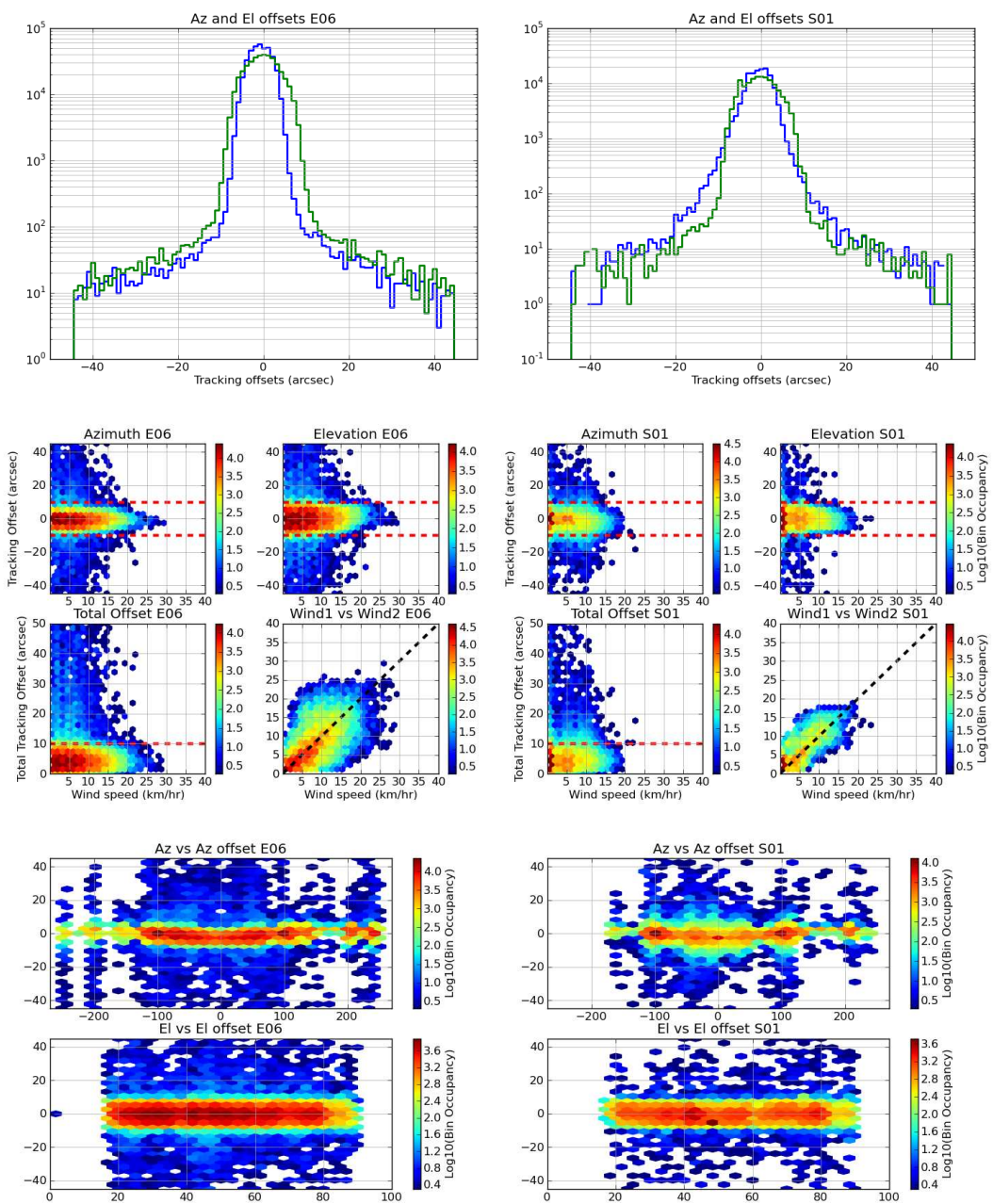
14

Figure 9: Figures for C06 and C08 in the same format as Fig. 6.

15

Figure 10: Figures for C09 and C10 in the same format as Fig. 6.

16

Figure 11: Figures for C11 and C12 in the same format as Fig. 6.

17

Figure 12: Figures for C13 and C14 in the same format as Fig. 6.

Figure 13: Figures for E02 and E03 in the same format as Fig. 6.

19

Figure 14: Figures for E04 and E05 in the same format as Fig. 6.

20

Figure 15: Figures for E06 and S01 in the same format as Fig. 6.

21
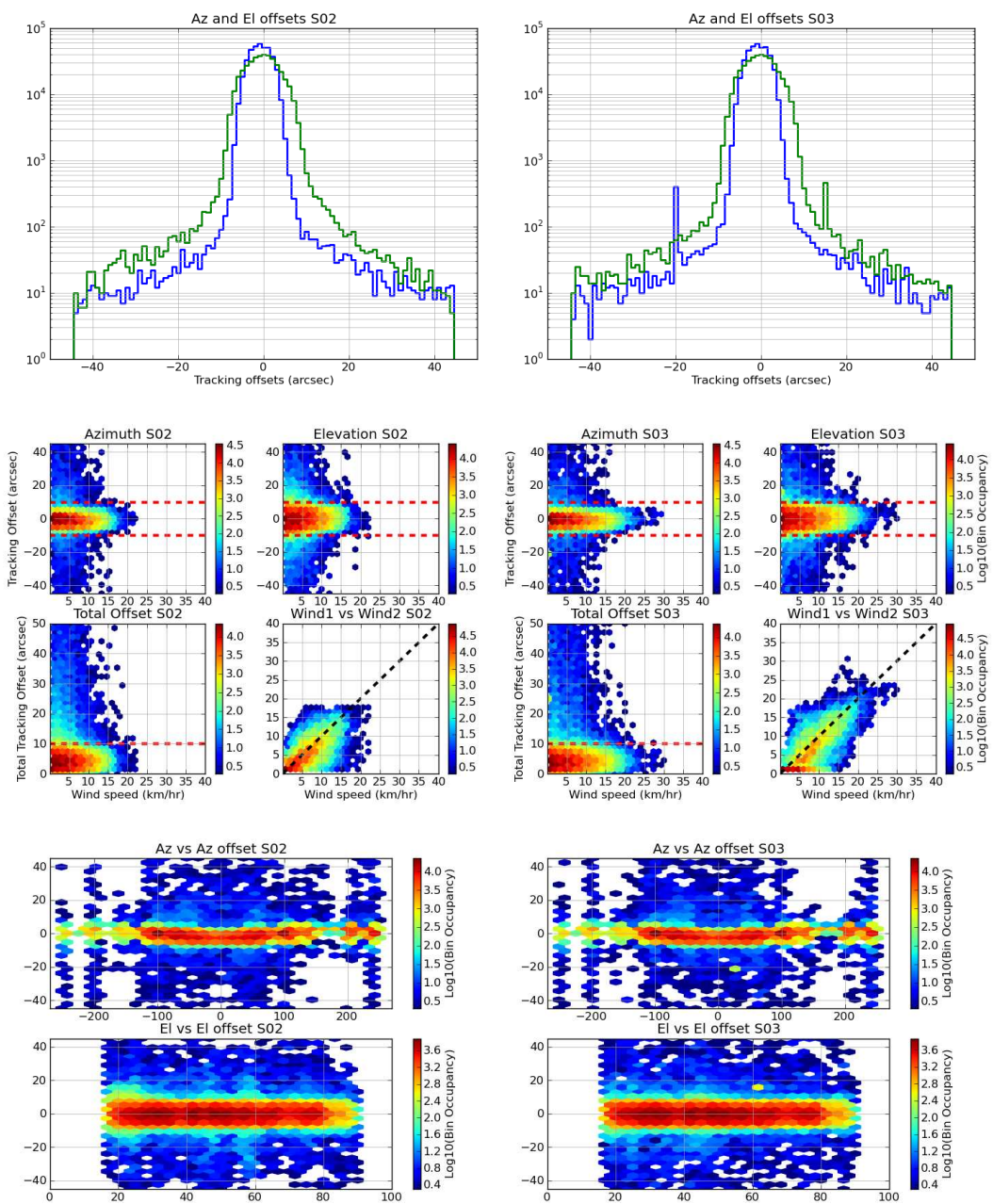
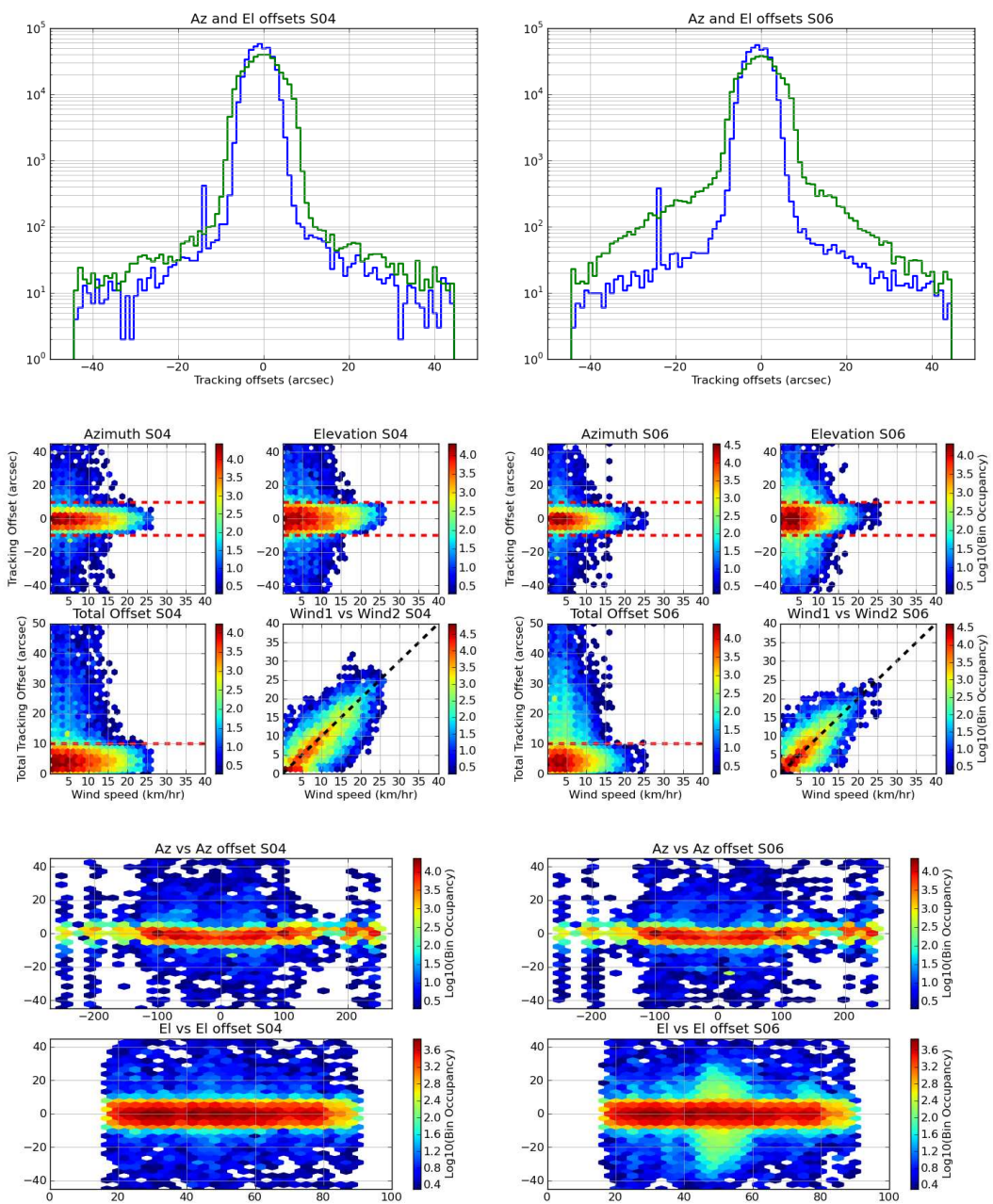Figure 16: Figures for S02 and S03 in the same format as Fig. 6.

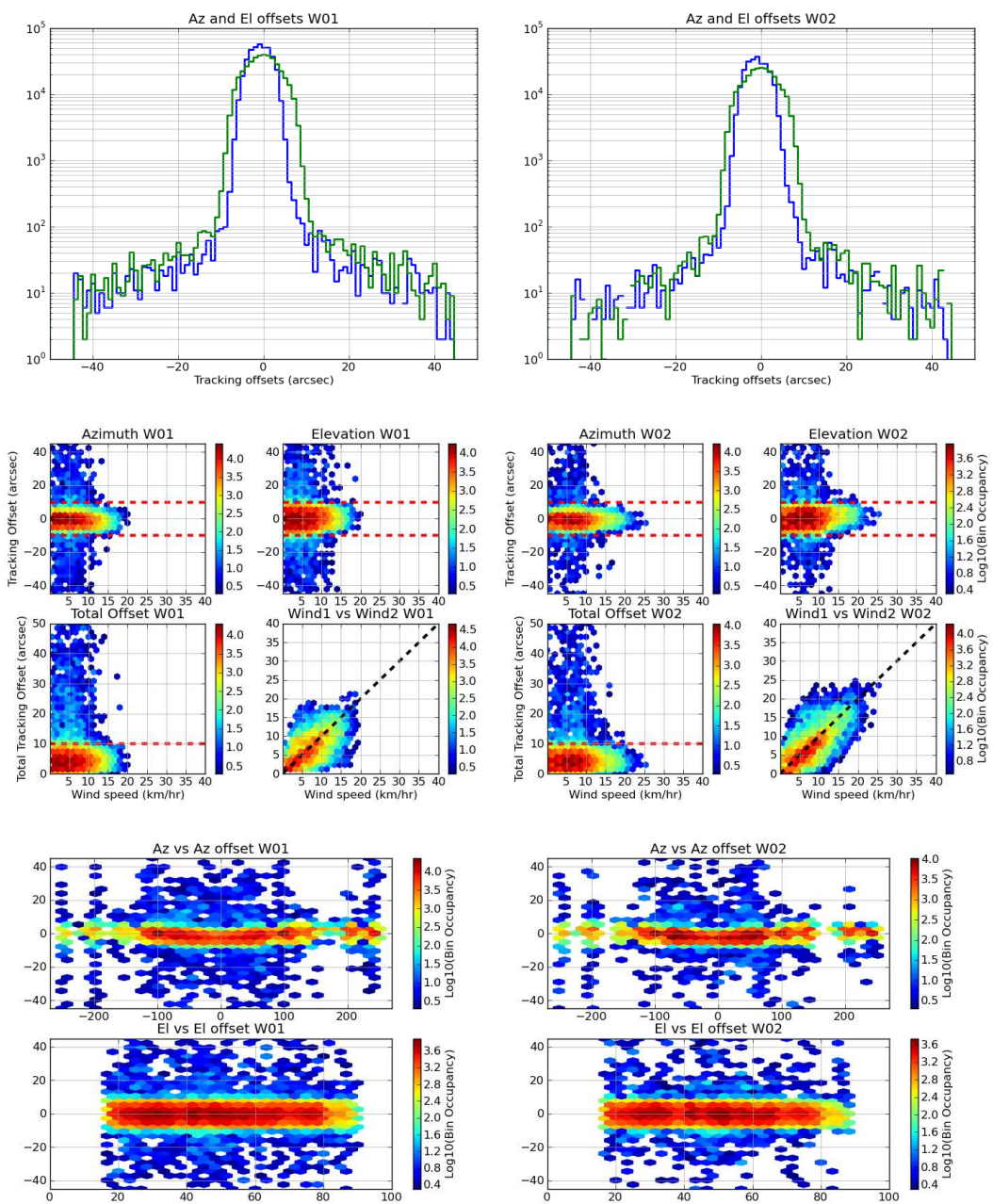Figure 17: Figures for S04 and S06 in the same format as Fig. 6.

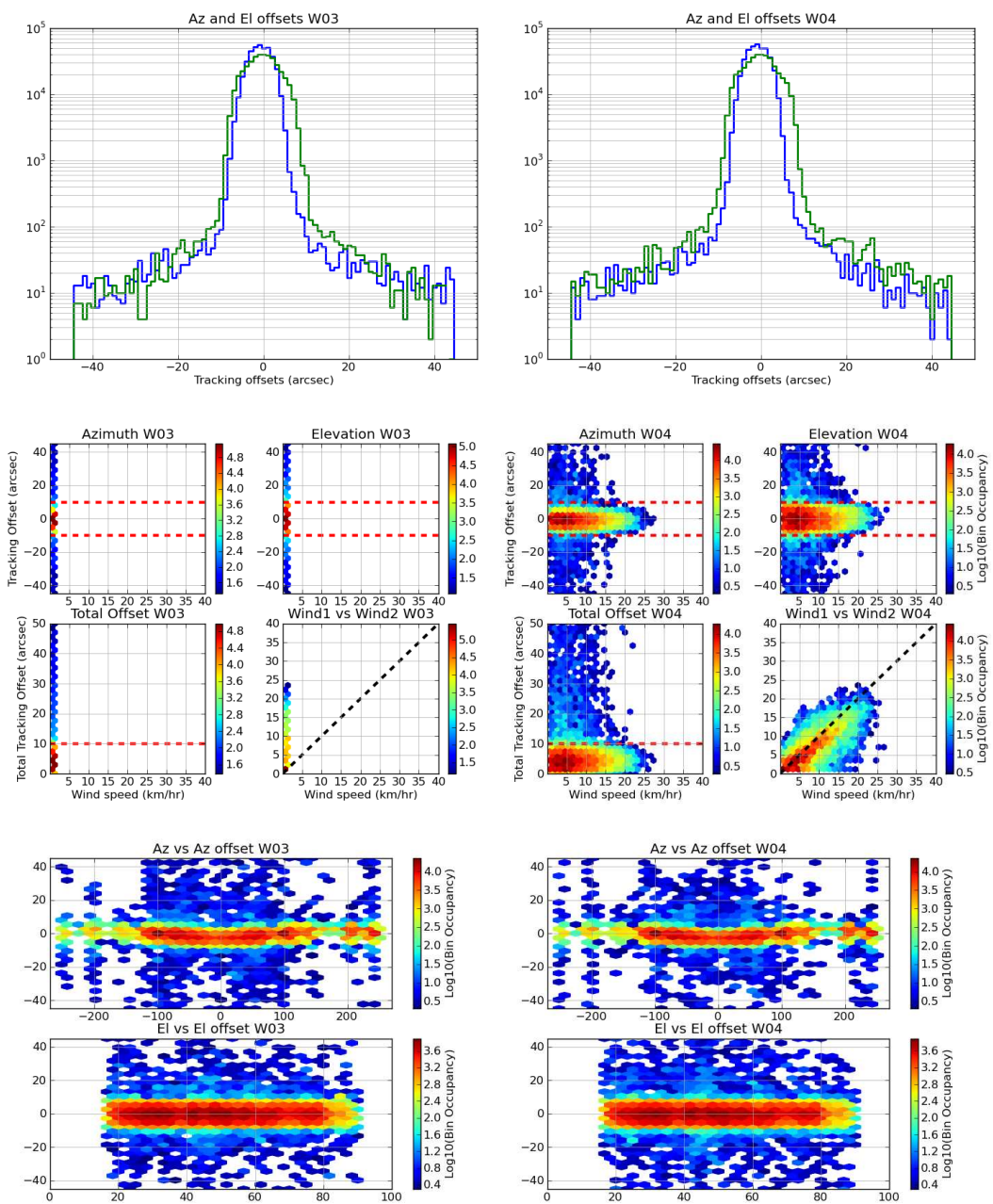Figure 18: Figures for W01 and W02 in the same format as Fig. 6.

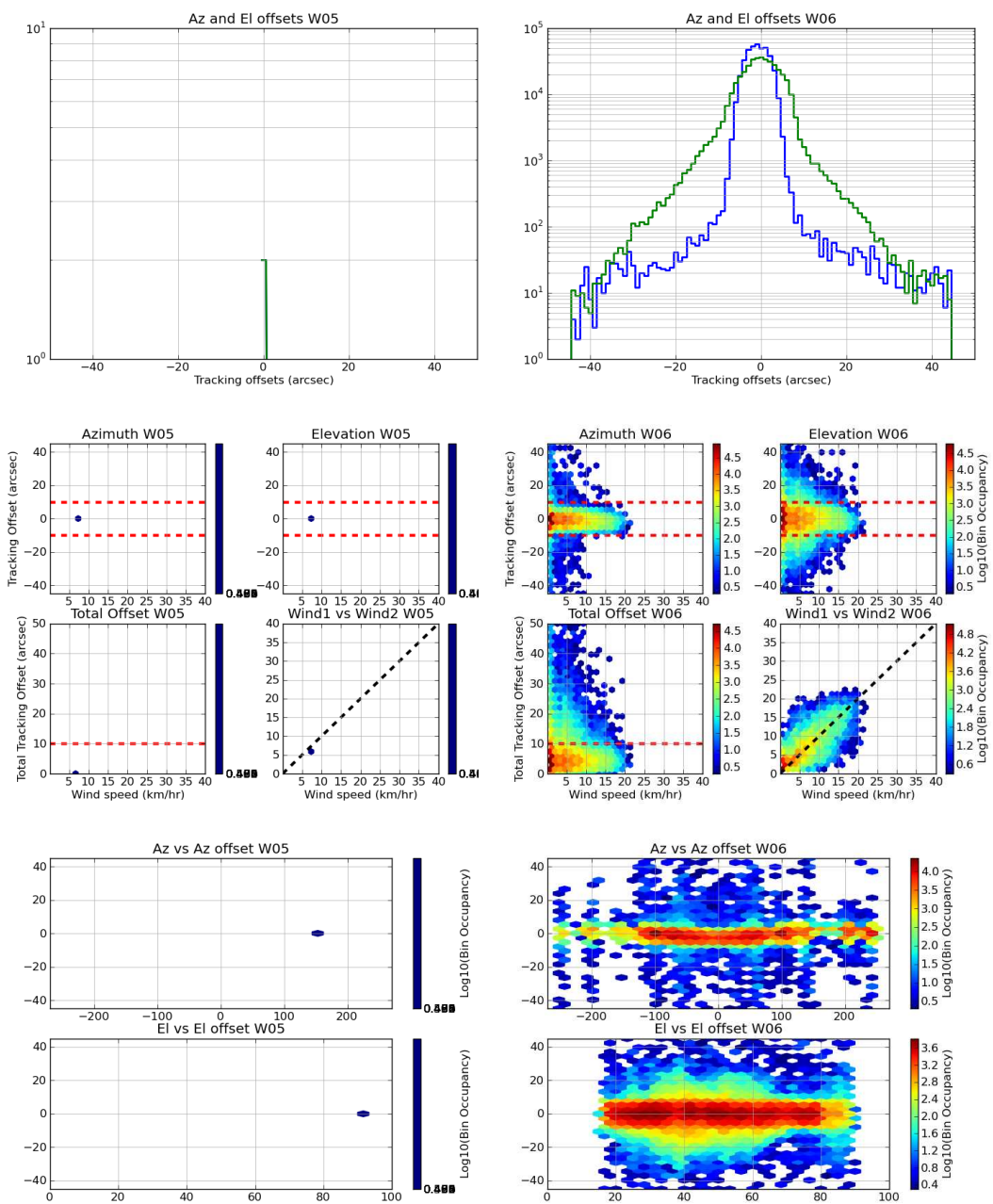Figure 19: Figures for W03 and W04 in the same format as Fig. 6.

Figure 20: Figures for W05 and W06 in the same format as Fig. 6.

26